Coherent Raman spectroscopy of nuclear quadrupole resonance of La around Pr^{3+} in LaF_3

Michio Matsushita*
Institute for Molecular Science, Okazaki, 444-8585, Japan

Akiko Mutoh†
School of Science, Kitasato University, Sagamihara, 228-8555, Japan

Tatsuhisa Kato
Institute for Molecular Science, Okazaki, 444-8585, Japan

(Received 24 April 1998; revised manuscript received 14 July 1998)

Coherent Raman spectroscopy was applied for an optical-rf double-resonance study of a LaF_3 crystal doped with Pr^{3+}. The coherent nuclear spin Raman scattering was detected as a function of the applied rf frequency. Exciting the resonance condition of the $^3H_4 \rightarrow {}^3P_0$ transition of Pr^{3+} (20 925 cm^{-1}), only the La nuclei surrounding the Pr^{3+} ion were observed through their nuclear quadrupole resonance (NQR). The double resonance between the optical transition of the ion and the NQR transition of its neighboring nucleus is theoretically described by analyzing the magnetic dipolar interaction that is affected by the optical excitation. Under a certain restriction, which the present system fulfills, the intensity of the Raman heterodyne signal can be described by an analytical function of the internuclear vector and the orientation of the electric-field gradient (EFG) at the Pr and La nuclei. Five different neighboring La nuclei were observed. They are different from the bulk La in both magnitude and orientation of the EFG. In addition, it was found that the laser frequency jitter affects the relative signal intensity of the different La NQR transitions through the optical pumping of the La spin levels. [S0163-1829(98)03145-2]

I. INTRODUCTION

Optical-magnetic double-resonance spectroscopy has been widely employed to detect magnetic dipole transitions of impurities in condensed media. The impurities are optically selected by resonant excitation of their optical transitions. One of the most popular methods called optically detected magnetic resonance (ODMR) utilizes saturation of optical transition. When a magnetic transition between spin sublevels modifies the population distribution in the optical process, the magnetic transition is optically detected as a change of the saturation. While ODMR monitors population, there are techniques manipulating coherence of the system. When the transverse relaxation of the optical transition is long enough, magnetic transitions can be observed as a change of the intensity of photon echo signal when the resonant rf is applied between the optical pulses. This method called photon echo nuclear double resonance observes optical coherence affected by population transfer of the spin system. In contrast, coherent Raman spectroscopy detects coherent excitation of the spin system by means of Raman scattering. It was demonstrated with coherent excitation of lattice vibrations[1] and later applied to a nuclear spin system.[2,3] Coherence of the spin system can be created by continuous or pulse rf irradiation as well as by optical pulse excitation. By combining with a probe laser field, the scattered field is detected as a heterodyne beat. The coherence of the scattering field manifests itself in various kinds of interference. These include site and Zeeman interference[4–7] and interference among different scattering pathways.[8] Because the scattering is a two-photon process involving magnetic spin- and optical electronic transitions, the coherence reflects properties of the spin system as well as the optical transition. Although it may become complicated, analysis of the interference can relate the magnetic parameters of the spin system to the optical transition dipole.

Following a series of coherent Raman spectroscopic studies of Pr^{3+} in LaF_3,[2,3,5–7,9] we had extended the study to the local environments around the impurity by observing the NQR transitions of La around the Pr^{3+} ion.[10] The appearance of La NQR in resonance Raman scattering of Pr^{3+} was qualitatively understood as due to the influence of the optical excitation on the magnetic dipolar interaction between the Pr and La nuclei. In the crystal the Pr^{3+} ion is surrounded by six inequivalent neighboring La atoms. Although those six La atoms are at about the same distance, only four La nuclei were observed. Quantitative investigation of the magnetic dipolar interaction should explain the observation of four out of six. Motivated by this we have developed a theoretical description of the Raman heterodyne signal. From the comparison between the experiment and the calculation, the local environments of neighboring La sites were found to be different from the bulk. In addition, the effect of the laser frequency jitter on the Raman heterodyne signal intensity was investigated.

II. THE SAMPLE

A. Crystal structure of LaF_3

There was a long controversy about the crystal structure of LaF_3 since the x-ray study in 1929,[11] but it has been now settled that the structure of LaF_3 is twinned $D_{3d}^4(P\bar{3}c1)$.[12,13] In the D_{3d}^4 structure the site symmetry of the La site is C_2.

The generating operations for the twins are those symmetry elements of $6/mmm\,(D_{6h})$ which are not contained in $\bar{3}m1$ (D_{3d}). For example, rotation of 180° about an axis parallel with c generates the second domain from the first one.

B. Spectroscopic properties of Pr^{3+} in LaF_3

From a rich spectroscopic knowledge about Pr^{3+} in LaF_3,[14] only the part necessary for our analysis will be presented here. The electronic ground state of Pr^{3+} is $^3H_4$. When embedded in the crystal, the ninefold degeneracy of $J=4$ is completely lifted due to the crystal field of C_2 symmetry. The lowest among the nine states is the ground state in the crystal. Although this ground state is an electronic singlet, since there are nonzero matrix elements of J between the states in the $^3H_4$ manifold, the second-order effect of the coupling between the electronic and magnetic angular momenta enhances the nuclear magnetic moment.[15] The enhancement over the bare nuclear moment (1.31 kHz/G) is large and anisotropic; the principal values of the effective nuclear moment are $(g_x,g_y,g_z)\beta/h = [4.98(4),2.53(3),10.16(3)]$ kHz/G.[16] The principal axes of the nuclear g tensor were found to coincide with those of the electric-field gradient (EFG) tensor. The y axis is parallel to the C_2 symmetry axis of the crystal field. Contrary to the ground state, there is no enhancement of the nuclear moment in the excited $^3P_0$ state of $J=0$. Upon the optical excitation the nuclear moment reduces, and consequently so does the magnetic dipolar interaction with the neighboring nuclei.

The zero-field quadrupole splittings in the ground state are 8.47 and 16.68 MHz. The parameters of the quadrupole Hamiltonian,

$$\mathcal{H}_Q = P\left[I_z^2 - \frac{1}{3}I(I+1) + \frac{\eta}{3}(I_x^2 - I_y^2)\right], \tag{1}$$

were most accurately determined in the coherent Raman experiment as $|P| = 4181.9(13)$ kHz and $\eta = 0.108(3)$.[3] The quadrupole splittings in the excited $^3P_0$ were observed as the envelope modulation of the photon-echo signal.[17] The splittings were 0.73 and 1.12 MHz, from which the quadrupole parameters were determined to be $|P| = 293$ kHz and $\eta = 0.516$. As in the case of the nuclear moment, the quadrupole interaction is enhanced in the ground state but it is not in the excited state. From the depth of the modulation, Chen, Chiang, and Hartmann[17] tried to determine the orientation of the excited state EFG tensor with respect to that in the ground state. However, partly due to the fact that the ground-state EFG tensor is nearly axial, it was difficult to determine the orientation uniquely.

C. Geometry of La around Pr^{3+}

As we will investigate closely, it is the magnetic dipolar interaction between the Pr and neighboring La nuclei that gives rise to the Raman heterodyne signal of the La NQR. Knowing the crystal structure and the magnetic parameters of Pr^{3+}, the analysis of the interaction will, in principle, give information about local magnetic environments of the neighboring La atoms. To prepare for the quantitative analysis, the internuclear vector will be calculated in this section.

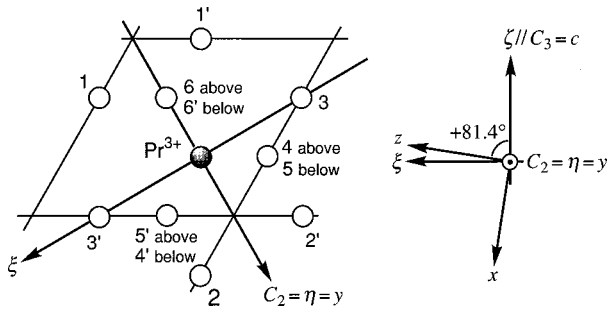

FIG. 1. Left: The LaF_3 crystal. Projection of rare-earth sites on a plane perpendicular to the crystal c axis. A central La site is replaced by Pr^{3+}. Due to the C_2 site symmetry, the 12 nearest-neighbor La atoms around the Pr^{3+} ion are classified into six pairs of equivalent atoms and they are labeled 1 and $1'$, 2 and $2'$, and so on. Right: Relation between the $\{\xi\eta\zeta\}$ axes and the principal $\{xyz\}$ axes of the Pr nuclear g and EFG tensors.

When the Pr^{3+} ion is doped into LaF_3 crystal, it replaces a La ion substitutionally in the lattice. A mixed crystal can be made at any concentration. The crystal structure of PrF_3 is also the twinned D_{3d}^4 (Ref. 18) and the lattice parameters differ by 1.5% from LaF_3,[11] so that the lattice distortion caused by doping is expected to be little. Therefore, we will use the parameters of LaF_3 itself. The cell dimensions of the crystal are $a = 7.185(1)$ Å and $c = 7.351(1)$ Å.[19] The atomic parameters of La are $x = 0.6598(1)$, $y = 0$, $z = 1/4$.[13] There are six La sites in the unit cell at $\pm(x,0,1/4;0,x,1/4;-x,-x,1/4)$. The lattice made by rare-earth sites resembles the hexagonal close-packed (hcp) structure where $x = 2/3$ and $c/a = 2/3\sqrt{(8/3)} = 1.089$. Thus, Pr^{3+} has 12 nearest-neighbor La atoms. Because of the site symmetry of C_2, the 12 La atoms are classified into six pairs of equivalent atoms. In Fig. 1 the six pairs are denoted by 1 and $1'$, 2 and $2'$, and so on. In the figure the η axis is the twofold symmetry axis of the Pr^{3+} site, the ζ axis is parallel to the threefold crystal c axis, and the ξ completes the orthogonal set of $\{\xi\eta\zeta\}$. To have a simple expression of the dipolar interaction, we will use the principal axis system $\{xyz\}$ which is common to the Pr g and EFG tensors. The relation between the $\{\xi\eta\zeta\}$ and $\{xyz\}$ axes is shown in the right-hand side of Fig. 1. The y axis is parallel to the η axis and the x and z axes are on the plane perpendicular to it. The z axis makes an angle of 81.4° with the ζ axis.[16] Depending upon the domain, the sign of this angle will be either positive or negative. Here we will fix it to be positive, i.e., the $\{\xi\eta\zeta\}$ axes are transformed into the $\{xyz\}$ axes by rotation defined by Euler angles of $(\alpha = \gamma = 0,\ \beta = +81.4°)$. In Table I the internuclear vectors of site 1–6 are represented by the distance r and the polar angles (ϕ,θ) on the $\{xyz\}$ system. Combined with the La nuclear moment (0.605 kHz/G) and the principal z value of the Pr nuclear moment (10.16 kHz/G) the internuclear distance gives the scale of the magnetic dipolar interaction between the two nuclei. The calculated factor for each La site is listed in the last column of the table.

To investigate the local magnetic environments of the neighboring La nuclei, we will start with the orientation of the principal $\{XYZ\}$ axes of the EFG tensor of the bulk La. The Y axis is along the C_2 symmetry axis of the site and the Z axis makes an angle of 53.6° with the c axis.[20] However, this will not give a unique orientation of the tensor. The

TABLE I. Internuclear vector between Pr^{3+} and six nearest-neighbor La's represented on the Pr g and EFG principal axis system $\{xyz\}$. The last column gives prefactor of the Pr-La dipolar interaction [see Eq. (16)], where $g_z(\mathrm{Pr})=10.16$ kHz/G and $g(\mathrm{La})=0.605$ kHz/G.

La site	r (Å)	ϕ (degrees)	θ (degrees)	$\frac{\mu_0\beta^2}{4\pi h}\frac{g_z(\mathrm{Pr})g(\mathrm{La})}{r^3}$ (kHz)
1	4.106	−84.86	59.36	0.589
2	4.234	85.07	60.37	0.537
3	4.106	173.14	171.34	0.589
4	4.414	162.81	110.47	0.474
5	4.414	20.23	126.78	0.474
6	4.334	−147.71	82.71	0.500

twinning of the crystal causes complications. The macroscopic observation of the La sites comprises contributions from two domains. As in the case of the Pr principal axes, the angle of Z from the c axis is positive in one domain and it is negative in the other domain. Since the relation between the angle and the domain is not established, orientation of the La tensor cannot be specified in the $\{xyz\}$ system. In other words, in the domain where the angle for Pr is +81.4°, we do not know whether the angle for La is +53.6° or −53.6°. If it is +53.6°, the Euler angles transforming the $\{xyz\}$ axes to the $\{XYZ\}$ axes are (+132.9°, +108.0°, −64.2°) for La 1, 2, 3, 4, and 5, and they are (0°, −27.8°, 0°) for La 6. If it is −53.6°, the Euler angles are (−127.1°, +60.9°, −78.6°) for La 1–5, and they are (0°, −135.0°, 0°) for La 6.

III. THEORY

This section is structured as follows. After a qualitative explanation of appearance of the La NQR in Pr^{3+} Raman scattering, several approximations will be introduced to make the treatment simple. Then, behavior of the coupled half-integer spin system of La ($I=7/2$) and Pr ($I=5/2$) will be investigated in detail. Finally the analytical expression will be derived to describe how the signal depends on the internuclear vector and the orientation of the EFG tensors of the two nuclei.

A. Appearance of La spin coherence in Pr^{3+} Raman scattering

The process of coherent Raman scattering is illustrated in Fig. 2. In our experiments continuous rf irradiation coherently drives the magnetic transition between states I and II.

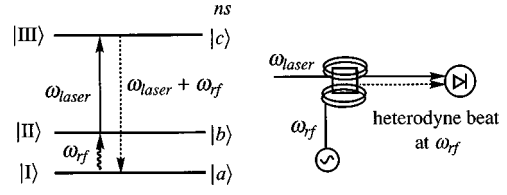

FIG. 2. Principle of heterodyne detection of coherent Raman scattering. Continuous rf and laser irradiation drive the magnetic transition I→II and the optical transition II→III. Because of the phase matching condition the Raman field (dotted arrow) propagates collinearly with the transmitted laser field (solid arrow). The Raman field is detected as a heterodyne beat of the transmitted light by a fast photodiode.

In addition a cw laser field drives the optical transition between II and III. The magnetic-optical two-photon process creates the second-order polarization between I and III, which emits the Raman field. Because the frequency of the magnetic transition is far smaller than the optical frequency, the phase matching condition makes the Raman field propagate in the same direction as the incident optical field. Since the Raman field is superposed on the transmitted laser field, the coherent Raman field E_S is detected as a heterodyne beat of the transmitted light by a fast photodiode (see right-hand side of Fig. 2). The beat frequency is the difference between the two optical fields, which is equal to the frequency of the applied rf. The amplitude and phase of the beat are expressed by a second-order susceptibility. Apart from the frequency-dependent denominator, the Raman field E_S is expressed as follows:[3]

$$E_S=\Delta n_{\mathrm{I,II}}\langle \mathrm{I}|\mu_B|\mathrm{II}\rangle\langle \mathrm{II}|\mu_E|\mathrm{III}\rangle\langle \mathrm{III}|\mu_E|\mathrm{I}\rangle, \tag{2}$$

where Δn represents the population difference, μ_B and μ_E denote the magnetic and the electronic transition moment operators, respectively. When the wave functions are separated into the electronic and the nuclear spin functions, the signal is represented by

$$E_S=\Delta n_{ab}|\mu_{\mathrm{opt}}|^2\mu_{ab}\langle b|c\rangle\langle c|a\rangle, \tag{3}$$

where $|a\rangle$ and $|b\rangle$ are the nuclear-spin functions in the electronic ground state and $|c\rangle$ is the nuclear-spin function in the electronic excited state. The optical transition moment is represented by μ_{opt} and magnetic transition moment between spin states $|a\rangle$ and $|b\rangle$ is represented by μ_{ab}. Because we fix the optical condition in resonant with the Pr^{3+} transition and measure NQR spectra as a function of rf frequency, we will focus our attention on the nuclear-spin part of the second-order susceptibility which will be denoted by χ_2,

$$\chi_2=\Delta n_{ab}\mu_{ab}\langle b|c\rangle\langle c|a\rangle. \tag{4}$$

Because the nuclear-spin system consists of weakly coupled Pr and La spins, the two spins can be treated separately in qualitative consideration. Since it is La NQR that is driven by rf, the Pr spin state is common to states $|a\rangle$ and $|b\rangle$. The Pr spin part in the overlapping factor $\langle b|c\rangle\langle c|a\rangle$ is simply the overlap between the ground and excited Pr spin functions. For the La spin, it stays basically the same when the Pr^{3+} ion is optically excited. The La spin state in $|c\rangle$ is very close to that in $|b\rangle$ so that the overlap $\langle b|c\rangle$ is close to unity.

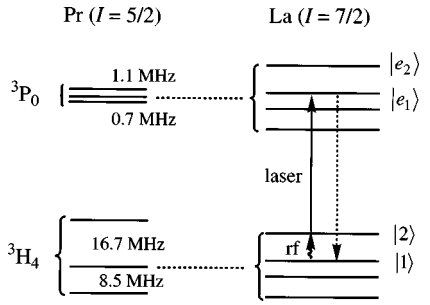

FIG. 3. Nuclear-spin levels of Pr and La associated with the Pr^{3+} $^3H_4 \rightarrow {}^3P_0$ transition. The arrow in the figure represents one of the scattering pathways for a La NQR transition of $|1\rangle \rightarrow |2\rangle$.

However, since the Pr-La magnetic dipolar interaction in the excited state is smaller than the ground-state interaction, the La state in $|c\rangle$ is slightly different from that in $|b\rangle$. This makes $|c\rangle$ carry a small character of $|a\rangle$ so that the overlap $\langle c|a\rangle$ becomes nonzero. Thus, the change of the magnetic interaction upon excitation is essential for observation of the Raman heterodyne signal. If the interaction was not affected by the excitation, the orthogonality between $|c\rangle$ and $|a\rangle$ would make χ_2 zero. To put it in a simple way, the neighboring La nuclear spin feels the optical excitation of Pr^{3+} through magnetic dipolar interaction with the Pr nucleus, because the Pr nuclear moment decreases upon the optical transition.

B. Approximations

As is discussed in the previous section the influence of the dipolar interaction on the Pr spin contributes little to the overlapping factor compared with the essential contribution from the La spin. Therefore we will ignore the effect of the dipolar interaction on the Pr spin states (Approximation I). As a result, the nuclear-spin states $|a\rangle$, $|b\rangle$, and $|c\rangle$ are written as a product of Pr and La spin functions

$$|a\rangle = |\mathrm{Pr};k\rangle|1\rangle, \tag{5a}$$

$$|b\rangle = |\mathrm{Pr};k\rangle|2\rangle, \tag{5b}$$

$$|c\rangle = |\mathrm{Pr}^*;l\rangle|e_i\rangle. \tag{5c}$$

$|\mathrm{Pr};k\rangle$ and $|\mathrm{Pr}^*;l\rangle$ are the eigenfunctions of Pr quadrupole Hamiltonian in the ground and in the excited state, respectively. $|1\rangle$ and $|2\rangle$ are the La spin functions in the ground state and $|e_i\rangle$ is the La spin function in the excited state. Because of the dipolar interaction they are linear combinations of the eigenfunctions of La quadrupole Hamiltonian. The nuclear-spin states of the Pr-La system associated with the Pr^{3+} $^3H_4 \rightarrow {}^3P_0$ transition are represented in Fig. 3.

When three La spin functions in the scattering process are fixed, there remains the freedom of Pr spin to be associated with; three in the ground state and three in the excited state. Since we do not know the EFG orientation in the excited state, we will average contributions from different scattering pathways via the three excited-state Pr spin states (Approximation II). In addition, since the dipolar interaction is about 8 times smaller in the excited state, we will ignore the dipolar interaction in the excited state (Approximation III). Then, the excited-state La spin function $|e_i\rangle$ becomes independent of the Pr spin. When the contributions from all the three pathways are summed up, we find

$$\begin{aligned}\sum_l \Delta n_{ab}\mu_{ab}\langle b|c\rangle\langle c|a\rangle &= \Delta n_{ab}\mu_{ab}\langle \mathrm{Pr};k|\langle 2|e_i\rangle \\ &\times\left(\sum_l |\mathrm{Pr}^*;l\rangle\langle \mathrm{Pr}^*;l|\right) \\ &\times\langle e_i|1\rangle|\mathrm{Pr};k\rangle \\ &= \Delta n_{ab}\mu_{ab}\langle 2|e_i\rangle\langle e_i|1\rangle.\end{aligned}$$

Since the Pr spin part in μ_{ab} gives unity for the La NQR transition, the nuclear-spin part of the susceptibility χ_2 is represented as

$$\chi_2 = \Delta n_{12}\langle 1|\mathcal{H}_{\mathrm{rf}}|2\rangle\langle 2|e_i\rangle\langle e_i|1\rangle, \tag{6}$$

where $\mathcal{H}_{\mathrm{rf}}$ denotes the rf transition moment operator for the La spin. Now the χ_2 is represented only by the La spin functions. Note, however, that the La spin states 1 and 2 depend on the ground-state Pr spin function through the ground-state dipolar interaction.

C. Raman heterodyne susceptibility and NQR frequency

A coherent Raman scattering pathway indicated in Fig. 3 involves the La NQR transition of $|1\rangle \rightarrow |2\rangle$ and optical transition of $|2\rangle \rightarrow |e_1\rangle$. The χ_2 for this pathway is written as follows:

$$\chi_2 = \Delta n_{12}\langle 1|\mathcal{H}_{\mathrm{rf}}|2\rangle\langle 2|e_1\rangle\langle e_1|1\rangle. \tag{7}$$

With slightly different laser frequencies, other resonant scattering pathways like the one involving optical transition of $|2\rangle$ to $|e_2\rangle$ will be activated also. The relation between the laser frequency jitter and the coherent Raman signals will be discussed later (see the Discussion). In calculating the transition moment, the La spin functions can be approximated as eigenfunctions of La quadrupole Hamiltonian denoted by $|i_0\rangle$,

$$\langle 1|\mathcal{H}_{\mathrm{rf}}|2\rangle \cong \langle 1_0|\mathcal{H}_{\mathrm{rf}}|2_0\rangle. \tag{8}$$

Because of Approximation III the La spin functions in the excited state are the eigenfunctions, i.e., $|e_1\rangle = |1_0\rangle$ and $|e_2\rangle = |2_0\rangle$. Since the Pr-La dipolar interaction is on the order of kHz and is far smaller than the quadrupole splitting on the order of MHz, it can be treated as a first-order perturbation. On the first order of the dipolar interaction, the overlapping factor is approximated as

$$\langle 2|e_1\rangle\langle e_1|1\rangle \cong \langle 2|e_1\rangle = \langle 2|1_0\rangle \cong \langle 2_0|\mathcal{H}_d|1_0\rangle/h\nu_0,$$

where $\mathcal{H}_d$ represents the ground-state dipolar interaction with the Pr spin and ν_0 is defined by the energy of state 2_0 measured from 1_0,

$$h\nu_0 = E(2_0) - E(1_0). \tag{9}$$

As a result the χ_2 is represented as follows:

$$\chi_2 = \frac{\Delta n_{12}}{h\nu_0}\langle 1_0|\mathcal{H}_{\mathrm{rf}}|2_0\rangle\langle 2_0|\mathcal{H}_d|1_0\rangle. \tag{10}$$

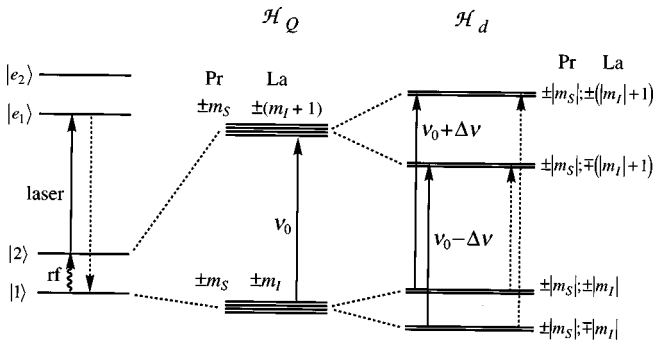

FIG. 4. The La NQR transition of the La-Pr spin system in the electronic ground state. The dipolar interaction $\mathcal{H}_d$ partially lifts the fourfold degeneracy of the states. The two solid arrows are the allowed La NQR transitions whereas the two dotted arrows are the forbidden transitions.

The diagonal matrix element of the dipolar interaction gives the first-order energy shift of La spin states. The NQR frequency ν is represented as

$$\nu=\left|\nu_0+\frac{1}{h}\left(\langle 2_0|\mathcal{H}_d|2_0\rangle-\langle 1_0|\mathcal{H}_d|1_0\rangle\right)\right|. \tag{11}$$

D. Dipolar coupled half-integer spins; La ($I=7/2$) and Pr ($I=5/2$)

Let us now construct the La spin functions in the ground state by taking account of the dipolar interaction with the Pr spin. In order to make the system as simple as possible, we will make two additional approximations; to assume axial symmetry for the ground-state Pr EFG (Approximation IV) and to assume axial symmetry for the La EFG tensor (Approximation V). Approximation IV may be a good one because the asymmetry parameter η is 0.108. However, Approximation V is not as good as IV, since the asymmetry parameter of La ranges from 0.54 to 0.84 (see Table III). The validity and limitations of this approximation will be discussed later (see the Discussion).

Because of these approximations the La and Pr spins are quantized along the symmetry axis of their EFG tensor. To make use of the diagonal representation in the azimuthal projection, the Pr and La spin operators are projected along their EFG principal axes, i.e., the (x,y,z) axes for Pr spin denoted by **S**, and the (X,Y,Z) axes for La spin denoted by **I**. Since the influence of the dipolar interaction on the Pr spin is ignored (Approximation I), terms containing ladder operators of Pr spin are discarded from $\mathcal{H}_d$. The truncated dipolar interaction and the rf transition moment take the following forms:

$$\mathcal{H}_d=S_z(pI_Z+qI_++q^*I_-), \tag{12}$$

$$\mathcal{H}_{\rm rf}=rI_Z+sI_++s^*I_-. \tag{13}$$

Let us consider the La NQR transition from $\pm|m_I|$ to $\pm(|m_I|+1)$ (see Fig. 4). When associated with a degenerate Pr level of $\pm|m_S|$, the upper and lower levels have fourfold degeneracy in the absence of dipolar interaction. If there is dipolar interaction among the degenerate states, the 4×4 matrix of the degenerate manifold must be diagonalized. For the truncated dipolar Hamiltonian of Eq. (12) this is only the case with $|m_I|=1/2$, because the ladder operators connect two states of $\Delta m_I=\pm1$. Therefore, within the present level of approximation, and except for $|m_I|=1/2$, the transition between the fourfold degenerate states can be treated as four independent transitions. When the first-order expression of the preceding section is applied, the NQR frequency shift $\Delta\nu$ and the nuclear-spin part of the second-order susceptibility of the coherent Raman process χ_2, become

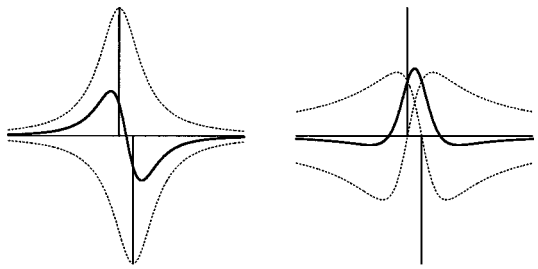

FIG. 5. The line shape of the Raman heterodyne signal. Left: When the phase of the detection is in absorptive mode, the superposition of the constituent absorption curves (dotted lines) results in a curve like dispersion. Right: When the phase is in dispersive mode, the superposition of the constituent dispersion curves results in a curve like a second derivative.

$$\Delta\nu=\nu-|\nu_0|=\pm\frac{\nu_0}{|\nu_0|}\,|m_S|\,\frac{p}{h}, \tag{14}$$

$$\chi_2=\pm i\,\frac{\Delta n_{12}}{h\nu_0}\,|m_S|\{I(I+1)-|m_I|(|m_I|+1)\}\mathrm{Im}(qs^*), \tag{15}$$

where the upper sign is for the two states where m_S and m_I have the same sign (parallel), and the lower sign is for the two states where m_S and m_I have the opposite sign (antiparallel). Note that in the absence of external magnetic field χ_2 is pure imaginary. This is consistent with the result of general consideration on the symmetry of the susceptibility with respect to the magnetic-field reversal,[21] where the coherent NMR Raman susceptibility $\sigma^{(3)}$ was shown to have the relation, $\sigma^{(3)}(-\mathbf{B})=-[\sigma^{(3)}(\mathbf{B})]^*$. Figure 5 summarizes the result with the line shape of the signal. The four degenerate transitions split into two doubly degenerate transitions. These two transitions have the same amplitude of the signal, but their phase is opposite to each other. Since the separation between the two transitions is smaller than the inhomogeneous broadening of the individual transitions (see the Discussion), the two transitions will not be resolved but overlap to give a single resonance line. The original expression of χ_2 of Eq. (6) tells that the Raman heterodyne signal is basically the La NQR weighted with the overlapping integrals. When the phase of the detection of the heterodyne beat is adjusted to absorptive mode, the resultant signal will look as if it was dispersion (see left-hand side of Fig. 5). When it is adjusted to the dispersive mode, the signal will look like a second derivative (right-hand side of Fig. 5). The resultant signal depends on both the amplitude of the two components $|\chi_2|$ and the separation between them $\Delta\nu$.

Incidentally, the Raman heterodyne signal does not depend on the sign of the quadrupole coupling constant P. A

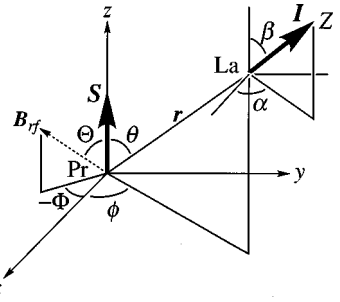

FIG. 6. La EFG tensor, internuclear vector between Pa and La, and rf field described on the Pr principal axis system {*xyz*}. The La EFG tensor is assumed to have axial symmetry. The angles α and β define the symmetry axis of the tensor. The polar angles (ϕ,θ) and (Φ,Θ) define the direction of the internuclear vector and the rf field, respectively.

positive coupling constant is assumed in the energy diagram of Fig. 4. There the larger the $|m_I|$, the higher the energy. When the coupling constant is negative, the energy diagram is reversed. By the definition of ν_0 [see Eq. (9)], ν_0 changes its sign, and both $\Delta\nu$ and χ_2 change their sign. Thus, the sign of the coupling constant has no influence on the line shape of the signal.

E. Dependence on the geometry and symmetry considerations

The next step is to describe the Hamiltonians $\mathcal{H}_d$ and $\mathcal{H}_{\rm rf}$ in terms of the internuclear vector, orientation of the EFG tensors, and the rf field. Figure 6 illustrates the relations of these angular quantities on the Pr principal axis system {*xyz*}. The direction of the internuclear vector and the rf field are represented by the polar angles (ϕ,θ) and (Φ,Θ), respectively. The Euler angles $(\alpha,\beta,0)$ define the translation from the {*xyz*} axes to the La principal axes {*XYZ*}. The third angle γ is fixed to zero, because the La EFG tensor is assumed to have axial symmetry. On the {*xyz*} system, truncated dipolar interaction and interaction with the rf field are represented as follows:

$$\mathcal{H}_d=\frac{\mu_0\beta^2}{4\pi}\frac{g_z(\mathrm{Pr})g(\mathrm{La})}{r^3}S_z \times\left\{(1-3\cos^2\theta)I_z-\frac{3}{4}\sin 2\theta(I^+e^{-i\phi}+I^-e^{+i\phi})\right\}, \tag{16}$$

$$\mathcal{H}_{\rm rf}=g(\mathrm{La})\beta B_{\rm rf}\left\{\cos\Theta I_z+\frac{1}{2}\sin\Theta(I^+e^{-i\Phi}+I^-e^{+i\Phi})\right\}, \tag{17}$$

where I_z, I^+, I^- denote components of La spin operators in the {*xyz*} system. Note that in the present level of approximation only the largest component of the Pr *g* tensor, $g_z(\mathrm{Pr})$, appears in the dipolar Hamiltonian. The La *g* tensor is isotropic because La^{3+} has an electronic closed-shell configuration. Using the following relation between (I_z, I^+, I^-) in the {*xyz*} system and (I_Z, I_+, I_-) in the {*XYZ*} system,

$$\begin{cases} I_z=\cos\beta I_Z-\dfrac{1}{2}\sin\beta(I_++I_-), \\ I^{\pm}=e^{\pm i\alpha}\left(\dfrac{\cos\beta+1}{2}I_{\pm}+\sin\beta I_Z+\dfrac{\cos\beta-1}{2}I_{\mp}\right), \end{cases} \tag{18}$$

we find the Hamiltonians of Eqs. (12) and (13) are now represented as

$$\mathcal{H}_d=\frac{\mu_0\beta^2}{4\pi}\frac{g_z(\mathrm{Pr})g(\mathrm{La})}{r^3}S_z(\tilde{p}I_Z+\tilde{q}I_++\tilde{q}^*I_-), \tag{19}$$

$$\mathcal{H}_{\rm rf}=g(\mathrm{La})\beta B_{\rm rf}(\tilde{r}I_Z+\tilde{s}I_++\tilde{s}^*I_-), \tag{20}$$

where

$$\tilde{p}=(1-3\cos^2\theta)\cos\beta-\frac{3}{2}\sin 2\theta\cos(\phi-\alpha)\sin\beta, \tag{21a}$$

$$\tilde{q}=-\frac{1}{2}(1-3\cos^2\theta)\sin\beta -\frac{3}{4}\sin 2\theta\{\cos(\phi-\alpha)\cos\beta-i\sin(\phi-\alpha)\}, \tag{21b}$$

$$\tilde{r}=\cos\Theta\cos\beta+\sin\Theta\cos(\Phi-\alpha)\sin\beta, \tag{21c}$$

$$\tilde{s}=-\frac{1}{2}\cos\Theta\sin\beta +\frac{1}{2}\sin\Theta\{\cos(\Phi-\alpha)\cos\beta-i\sin(\Phi-\alpha)\}. \tag{21d}$$

Before finishing simply with substitution of the angular parameters into $\Delta\nu$ and χ_2, let us consider some of the symmetry properties of the Raman heterodyne signal. For a pair of equivalent La nuclei around Pr^{3+}, the second site is generated from the first one by 180° rotation around the twofold *y* axis. Instead of rotating the La atom around the Pr^{3+} ion it is easier to rotate the external rf field and keep the orientation of the atoms. This leaves $\mathcal{H}_d$ intact and we only need to consider the rf direction in $\mathcal{H}_{\rm rf}$. Recalling that $\mathcal{H}_{\rm rf}$ is a magnetic transition moment proportional to $\mathbf{B}_{\rm rf}\cdot\mathbf{I}$, one sees that upon the C_{2y} operation on the rf field, $\mathcal{H}_{\rm rf}$ is symmetric for $\mathbf{B}_{\rm rf}\|y$ and it is antisymmetric for $\mathbf{B}_{\rm rf}\perp y$. Since the direction of the rf field affects χ_2 through $\mathcal{H}_{\rm rf}$ [see Eq. (6)], the pattern of the Raman heterodyne signal behaves in the same manner as $\mathcal{H}_{\rm rf}$, that is, upon the exchange of the equivalent La sites, the signal is symmetric for $\mathbf{B}_{\rm rf}\|y$ and it is antisymmetric for $\mathbf{B}_{\rm rf}\perp y$. This is one of those examples of site interference that can be understood by geometrical symmetry.[7] Another symmetry relation is about the twinning. The twin is generated by 180° rotation around an axis parallel with the *c* axis. Again, instead of rotating the crystal structure, rotation of the rf field will tell the relation between the signals of the two domains. Upon the exchange of the two domains the Raman

TABLE II. Symmetry relations of the Raman heterodyne NQR signal of La around Pr^{3+} in LaF_3.

rf field direction	C_2 equivalent sites Site $i \leftrightarrow$ site i'	Twinning Domain $A \leftrightarrow$ domain B
$\mathbf{B}_{rf} \| y$	Even	Odd
$\mathbf{B}_{rf} \| \xi$	Odd	Odd
$\mathbf{B}_{rf} \| c$	Odd	Even

heterodyne signal is symmetric for $\mathbf{B}_{rf} \| c$ and it is antisymmetric for $\mathbf{B}_{rf} \perp c$. The results of the symmetry relations are summarized in Table II.

Unless the external magnetic field is applied, the signals from the two equivalent sites overlap with each other. From the symmetry relations only the rf field along the y axis produces nonzero Raman signal. Therefore, we will fix the direction of the rf field to be parallel with the y axis and set $\Phi = \Theta = \pi/2$. By using the expressions of $\tilde{p}$, $\tilde{q}$, and $\tilde{s}$ of Eq. (21), the NQR frequency shift $\Delta\nu$ and the susceptibility χ_2 of Eqs. (14) and (15) are represented as

$$\Delta\nu = \frac{\mp\nu_0}{|\nu_0|}\frac{\mu_0\beta^2}{4\pi h}\frac{g_z(\mathrm{Pr})g(\mathrm{La})}{r^3}\frac{|m_S|}{2} \times\{(1+3\cos 2\theta)\cos\beta + 3\sin 2\theta\cos(\phi-\alpha)\sin\beta\}, \quad (22)$$

$$\chi_2 = \pm i\frac{\mu_0\beta^2}{32\pi h}\frac{g_z(\mathrm{Pr})g(\mathrm{La})^2 B_{rf\|y}}{\nu_0 r^3} \times\Delta n_{12}|m_S|\{I(I+1)-|m_I|(|m_I|+1)\}\times I_2, \quad (23)$$

where

$$I_2 = (1+3\cos 2\theta)\cos\alpha\sin\beta - 3\sin 2\theta\cos\phi\cos\beta. \quad (24)$$

Table I gives the internuclear vector and the scalar prefactor in the expression of $\Delta\nu$ for six nearest-neighbor La atoms around Pr^{3+}. As long as the approximations are good enough, the perturbation approach has an advantage to describe the signal analytically as a function of the unknown parameter of the orientation of the La EFG tensor.

IV. EXPERIMENT

The output from a cw single-mode ring dye laser (Coherent 899-29, dye: Coumarin 102) at 20 925.4 cm^{-1} was focused on the crystal to a diameter of about 100 μm with a power of 1–5 mW. The propagation direction of the laser field was parallel with the crystal c axis and the rf field was applied perpendicular to it. The LaF_3 crystal doped with 0.1 at. % Pr^{3+} (Optovac) is 5 mm thick along the c axis. The crystal was immersed in a liquid-He bath which was kept at 1.5 K. To perform the phase-sensitive detection of the rf signal, a network analyzer (hp 8752C) was used for an rf source and detection. After amplified to +20 dBm, the rf was applied to the crystal through a 10 turn coil. The inductance of the coil is about 1 μH. The heterodyne beat between the coherent Raman and the transmitted laser fields was detected by a photoreceiver with a bandwidth of 125 MHz (New Focus 1801-AC). The rf beat signal from the photodiode was sent to the network analyzer. The network analyzer detects the amplitude and phase of the signal with respect to the applied rf. The total electric length and the frequency-dependent phase delay at the coil were corrected to get a proper phase of the spectra. The signal was averaged over 6000–9000 scans.

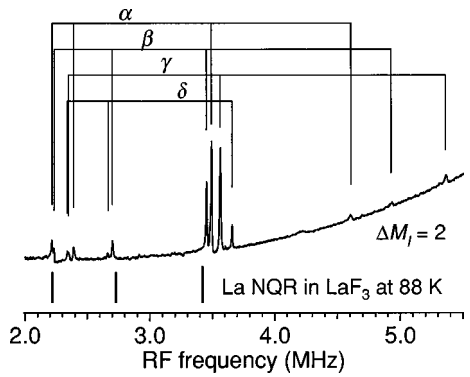

FIG. 7. NQR of La around Pr^{3+} in LaF_3 observed as a Raman heterodyne signal at 1.5 K. The $^3H_4 \rightarrow {}^3P_0$ transition of Pr^{3+} at 20 925 cm^{-1} was excited by a cw single-mode dye laser. The frequency jitter of the laser was about 3 MHz. The signals are assigned to four neighboring La atoms, α through δ.

The laser frequency was stabilized by locking it to a home-built 25 cm confocal etalon (FSR=300 MHz, finesse=30) using the method of Hänsch and Couillaud.[22] The error signal was sent to the commercial electronic control box of the ring laser. The laser frequency jitter was measured with a temperature-stabilized scanning confocal etalon (burleigh CFT-500-VIS, FSR=150 MHz, finesse=100).

V. RESULTS AND DISCUSSION

A. Observation of the La NQR around Pr^{3+}

Figure 7 shows the NQR signals of La around Pr^{3+} detected by coherent Raman scattering at 1.5 K. The laser was operated with the commercial stabilization system and the frequency jitter was about 3 MHz on the time scale of 0.1 s. As shown in the theoretical derivation, the second-order susceptibility of the coherent Raman process is pure imaginary. This means that when the phase correction is properly made over the entire frequency range, all the peaks should appear either in dispersive or absorptive shape, as is the case with Fig. 7. Because of the C_2 site symmetry only the rf field parallel with the twofold y axis produces nonzero Raman signal. According to symmetry relation about the twinning of the crystal, this nonzero Raman signal is opposite in phase in the two domains (see Table II). In accordance with this symmetry property, when the laser spot was scanned over the crystal, once in a while all the signals simultaneously change their phase by π, which means the laser beam crossed from one domain to the other. There are also regions where signals are very weak, which means the volume of the two domains that the laser beam probes is almost equal. The behavior is similar to that observed in the Raman heterodyne signal of the Pr NQR transition.[9]

As shown in Fig. 7 the signals were assigned to four different neighboring La, α through δ.[10] Three signals above

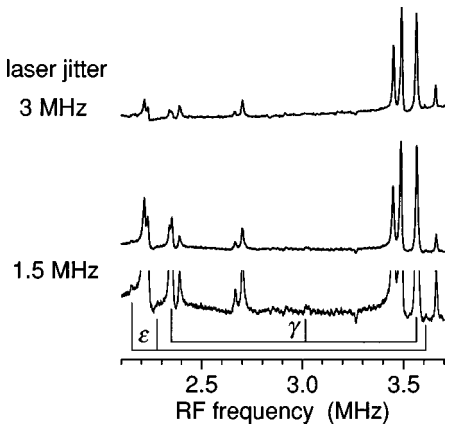

FIG. 8. Influence of the laser frequency jitter on the Raman heterodyne signals. Comparison of the spectra between jitter of 3 MHz (top) and 1.5 MHz (middle). The expanded spectrum with jitter of 1.5 MHz (bottom) shows several reproducible weaker transitions; One at 3013 kHz is assigned to the 1/2–3/2 transition of La γ. Three transitions at 2152, 2277, and 3605 kHz are assigned to the fifth La, ε.

4.5 MHz turned out to be forbidden transitions of $\Delta m_I = 2$. Since their frequency is the sum of the frequency of two allowed transitions, assignment of the signals of three La sites, α, β, and γ was unequivocal. A forbidden transition of the fourth La, δ, was not observed. The transition frequencies of the bulk La at 88 K (Ref. 23) are indicated in the figure for reference.

As for the magnetic transition moment, which the normal NQR detects, the intensity distribution among the allowed transitions of $\Delta m_I = \pm 1$ is such that the larger the $|m_I|$ the weaker the intensity. In the Raman heterodyne signal, the energy denominator of ν_0 in the expression of χ_2 also adds to this tendency, because the transition frequency $|\nu_0|$ is larger for a larger $|m_I|$. Thus, the 5/2–7/2 transitions at highest frequency around 3.5 MHz are expected to be the weakest among the allowed transitions. However, they are the strongest observed.

One of the factors we have not taken into account is the population. Although the effect is indirect, the continuous pumping of the optical transition of Pr^{3+} may cause the neighboring La spin to deviate from thermal equilibrium. No measurements were made on the spin-lattice relaxation of the neighboring La, but we could assume a similar relaxation time to the Pr spin, which is on the order of 1 s.[24] Since the laser frequency fluctuates 3 MHz on a comparable time scale with the relaxation time, the La NQR transitions lower than 3 MHz may be affected by the optical pumping effect. The frequency jitter was reduced to 1.5 MHz to investigate the effect of the laser jitter on the relative signal intensity of different transitions.

B. Influence of the laser frequency jitter

Figure 8 compares the Raman heterodyne spectra at different laser frequency jitters. When the jitter was reduced from 3 to 1.5 MHz, the 3/2–5/2 transitions around 2.2 MHz became stronger with respect to the strongest 5/2–7/2 transitions around 3.5 MHz. Evidently, the frequency jitter of cw laser irradiation affects the population of La spin levels.

The optical pumping effect can be qualitatively explained in the following way. Out of the inhomogeneously distributed ensemble of atoms, let us focus our attention on a particular set that have the same optical transition energy as the one depicted in Fig. 3, where the laser is in resonance with the optical transition from $|2\rangle$ to $|e_1\rangle$. If the laser frequency shifts slightly higher, the laser will be resonant with the transitions from $|1\rangle$ to $|e_1\rangle$ and $|2\rangle$ to $|e_2\rangle$. Since the excited-state La spin functions $|e_1\rangle$ and $|e_2\rangle$ are very close to the ground-state functions $|1\rangle$ and $|2\rangle$, respectively, these two optical transitions have much higher transition probability than the $|2\rangle - |e_1\rangle$ transition. The pair of these allowed optical transitions will contribute to the optical pumping effect through $|\Delta m_I| \neq 0$ relaxation. Direct radiative relaxation to the ground state with $|\Delta m_I| \neq 0$ is as forbidden as the optical absorption of the forbidden $|\Delta m_I| \neq 0$ transitions, but there is a considerable contribution of indirect multistep relaxation through intermediate states. About half of the emission from the $^3P_0$ state is to intermediate states like $^3H_6$ and $^3F_4$.[25] Since these intermediate states have the hyperfine coupling with the electronic angular momentum, the probability of the $|\Delta m_I| \neq 0$ transition would be larger than the direct process.[26] Therefore, when the atoms are excited through the pair of the allowed optical transitions, the optical pumping will equalize the population of the La spin levels $|1\rangle$ and $|2\rangle$.

When the laser excites the pair of the allowed transitions, the Raman signal is a superposition of simultaneous excitation of two scattering pathways, one involves the rf transition from $|1\rangle$ to $|2\rangle$ and the $|2\rangle - |e_2\rangle$ excitation, the other involves the rf transition from $|2\rangle$ to $|1\rangle$ and the $|1\rangle - |e_1\rangle$ excitation. The susceptibilities for the two pathways are expressed as follows:

$$\chi_2(12e_2) = \Delta n_{12} \langle 1|\mathcal{H}_{\rm rf}|2\rangle \langle 2|e_2\rangle \langle e_2|1\rangle,$$

$$\chi_2(21e_1) = \Delta n_{21} \langle 2|\mathcal{H}_{\rm rf}|1\rangle \langle 1|e_1\rangle \langle e_1|2\rangle.$$

When the overlapping factors are calculated using the first-order perturbation in the same way as in Eq. (10), we will find the susceptibilities of the two pathways are complex conjugate of each other, $\chi_2(12e_2) = \chi_2(21e_1)^*$. Recalling that the susceptibility in the zero magnetic field is pure imaginary [see Eq. (15) and Ref. 21], the superposition of the simultaneously excited two pathways will result in complete cancellation.

In summary, the Raman heterodyne signal is generated by exciting the forbidden optical transition. When the laser frequency shifts to excite the pair of the allowed optical transitions, the excitation will not produce coherent Raman signal, but will contribute to the optical pumping of the La spin levels to equalize the population of the levels $|1\rangle$ and $|2\rangle$. When the laser frequency shifts back and forth between the allowed and the forbidden transitions within the time scale of the spin-lattice relaxation, the excitation of the forbidden transition will create the coherent Raman signal, but with a smaller amplitude due to the reduced population factor Δn_{12}. The same argument applies to the excitation of the other forbidden transition from $|1\rangle$ to $|e_2\rangle$.

In the spectrum taken with a reduced laser jitter, the 5/2–7/2 transitions are still the strongest. Probably the reduction of laser jitter is not sufficient to suppress the optical pumping effect completely. Another possibility is the incomplete

TABLE III. Quadrupole parameters of La around Pr^{3+} in LaF_3 at 1.5 K. The parameters of the bulk La in LaF_3 are also included for reference.

La ($I=7/2$)	$\lvert P\rvert$ (kHz)	η
α[a]	609.0(4)	0.650(1)
β[a]	613.5(4)	0.765(1)
γ[a]	641.8(4)	0.835(3)
δ[a]	643.6(4)	0.703(2)
ε[b]	619.7(9)	0.540(5)
Bulk at 88 K[c]	610.0(4)	0.7845(10)

[a]Reference 10.
[b]Present work.
[c]Reference 23.

treatment of the excited state because of the lack of information on the orientation of the excited-state Pr EFG tensor.

With the increased sensitivity at lower frequencies, several weak signals were found to be reproducible. One at 3013(9) kHz is assigned to the 1/2–3/2 transition of La γ predicted at 3010 kHz.[10] Two signals at 2152(12) and 2277(11) kHz, together with a signal at 3605(5) kHz which was already evident in the spectrum taken with a larger laser jitter, fit to the quadrupole splitting pattern of spin-7/2 system. The parameters $|P|=619.7$ kHz and $\eta=0.540$ give transitions at 2151, 2278, and 3605 kHz. They can be assigned to the fifth neighboring La, ε, as indicated in Fig. 8. The parameters of La α–ε are summarized in Table III.

C. Validity of the perturbation calculation

Although the Pr^{3+} ion is surrounded by six inequivalent nearest-neighbor La atoms, only four La atoms contribute the major signals to the coherent Raman scattering. Since the distance is about the same for the six neighbors, the intensity reflects the orientation of the EFG at individual La sites. The relation between the orientation and the signal was given by the perturbation approach described in the theoretical section. However, one should keep in mind that five approximations were introduced in the course of the derivation. Especially Approximation V that assumes axial symmetry of the La EFG is a poor one. Therefore, the validity and limitations of the approximations must be evaluated before applying the results. To that end the χ_2 and $\Delta\nu$ were calculated by diagonalizing the ground-state dipolar interaction. The treatment of the ground state is exact and the remaining approximations are those concerning the excited state, to average the contributions from the scattering pathways through the three excited-state Pr spin states (Approximation II), and to ignore the dipolar interaction in the excited state (Approximation III).

Figure 9 compares the results of the perturbation and the diagonalization of La γ which has the largest asymmetry parameter $\eta=0.835$. In the perturbation treatment, a single La transition of $|m_I|\leftrightarrow|m_I|+1$ consists of three pairs of transitions corresponding to Pr spin states of $m_S=\pm1/2$, $\pm3/2$, and $\pm5/2$. Because both $\Delta\nu$ and χ_2 are proportional to $|m_S|$ [see Eqs. (14) and (15)], the three La transitions have the same pattern of three pairs (see upper part of Fig. 9). Since $\Delta\nu$ is independent of $|m_I|$, the width of the pattern is the same for all the three transitions, while the factor $\{63/4-|m_I|(|m_I|+1)\}/\nu_0$ determines the intensity of the pattern of each La transition. The transitions with $|\Delta m_I|>1$ or $|\Delta m_S|\neq0$ are indicated by dotted line in Fig. 4. Because of the axial symmetry of the EFG and the first-order treatment, those transitions are strictly forbidden and do not appear in the perturbation. In the result of the diagonalization, however, they have finite intensity in the periphery of the patterns (see lower part of Fig. 9). In nonaxial quadrupole interaction the mixing of the $|m_I\rangle$ basis functions is stronger in a lower $|m_I|$ state. Furthermore, as mentioned during the derivation, the nondegenerate perturbation is not applicable to the lowest $|m_I|=1/2$ states. As a consequence the perturbation gives the best result in the 5/2–7/2 transition. The same argument applies to the $|m_S|$ of the Pr spin. When we look into the details of the $|m_S|$ manifold of the 5/2–7/2 transition, we find that the smaller the $|m_S|$, the larger the discrepancy. However, because it is the influence of the neighbor spin on the La transition, and because the Pr EFG is more axial, the discrepancy is not crucial.

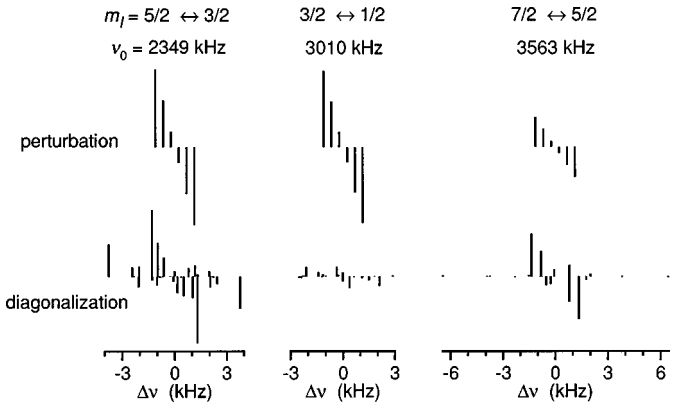

FIG. 9. Calculation of the coherent Raman signal of the La NQR transitions. Comparison between the perturbation and the diagonalization of the ground-state dipolar interaction. The calculation uses the quadrupole parameters of La γ and the internuclear vector of site 6. The Z axis is chosen to be $-53.6°$ from the crystal c axis, which is one of the two possible EFG orientations of the bulk La.

D. Calculation of intensity of the 5/2–7/2 transition

From the comparison of the stick diagrams in Fig. 9, the perturbation expression seems applicable to the 5/2–7/2 transition. To estimate the observed signal intensity, the perturbation and the diagonalization must be compared in a resonance line averaged over the dipolar broadening due to the surrounding F nuclei. Since the nuclear magnetic moment roughly scales with the dipolar broadening, the dipolar width can be estimated from the linewidth of the Pr NQR transition of 160 kHz.[3] From the ratio of the nuclear moments between $g_z(\mathrm{Pr})=10.16$ and $g(\mathrm{La})=0.605$ kHz/G, the dipolar width due to La-F interaction is estimated to be 9 kHz. The value agrees with the linewidth of the La NQR transitions of about 10 kHz, since additional broadening due to the La-Pr interaction is expected to be small. To get an absorptive line shape the components must be convoluted with the dispersion curve (see Fig. 5). As for the stick diagram of the diagonalization all the components of the 5/2–7/2 transition

were convoluted with the dispersion curve of linewidth of 9 kHz. As for the perturbation, we took a simple process by approximating the dispersion curve to be linear within the region of $\Delta\nu$. Since Eq. (22) estimates the maximum $\Delta\nu$ of 2.9 kHz, the approximation becomes poor when $\Delta\nu$ is large. However, the advantage is that the peak height of the resonance curve becomes proportional to the product of the shift $\Delta\nu$ and the susceptibility χ_2. The product of $\Delta\nu$ and χ_2 was calculated for 12 different sets of parameters, i.e., two possible EFG orientations of the bulk La at each of six La sites, and the intensity distribution over the 12 products was compared with the proper convolution of the result of diagonalization. Despite the simplifications, the pattern obtained by the product of $\Delta\nu$ and χ_2 agrees with the convolution of the stick diagram of diagonalization. The difference is within 3% of the largest signal.

In conclusion the geometrical dependence of the intensity of the Raman heterodyne signal is represented by the product of $\Delta\nu$ and χ_2. The expression is given as follows:

$$I_{\mathrm{RHS}}(5/2\rightarrow 7/2)\propto\chi_2\Delta\nu\propto\frac{1}{r^6}\times S, \tag{25}$$

$$S=B-C\ \sin 2\alpha-B\ \cos 2\alpha+(A\ \sin\ \alpha+D\ \cos\ \alpha)\sin 2\beta$$
$$+(3B+C\ \sin 2\alpha+B\ \cos 2\alpha)\cos 2\beta, \tag{26}$$

where

$$A=9\ \sin^2 2\theta\ \sin 2\phi, \tag{27a}$$

$$B=3(1+3\ \cos 2\theta)\sin 2\theta\ \cos\ \phi, \tag{27b}$$

$$C=3(1+3\ \cos 2\theta)\sin 2\theta\ \sin\ \phi, \tag{27c}$$

$$D=18\ \sin^2 2\theta\ \cos^2\phi-2(1+3\ \cos 2\theta)^2. \tag{27d}$$

E. Local La environments around Pr^{3+}

The spectra of neighboring La NQR are the most interesting from the viewpoint of the local environment around the Pr^{3+} ion. As is obvious from the NQR frequency the local electric-field gradient (EFG) is clearly different from the bulk. What about its orientation? Let us compare the observation with what is expected for the environment of the bulk. Using the Eqs. (25)–(27) the signal intensity of the 5/2–7/2 transition is calculated for the six La sites. The result is shown by thick bars in Fig. 10. As is mentioned earlier, there are two possible EFG orientations of the bulk La. In the experimental spectra, the four 5/2–7/2 transitions around 3.5 MHz are all in the same phase. The calculation shows that La site 3 gives the largest signal amplitude, but it is opposite in phase to the next strongest ones. Both of the two orientations of the bulk La cannot reproduce the observation. The discrepancy indicates that the EFG tensors of the neighboring La atoms are rotated away from the orientation of the bulk. Since the intensity ratio between La sites could at most compare the relative orientation of the tensor at one site with respect to the other, we cannot determine the absolute EFG orientation in the crystal. Nevertheless, the analytical expression of Eq. (26) can provide the maximum signal amplitude that each site can produce. The result is shown by thin lines in Fig. 10. The possible maximum amplitude is the largest at site 3. Site 1 and 2 are smaller than the others. The sites giving major signals of α, β, γ, and δ are most probably site 3, 4, 5, and 6.

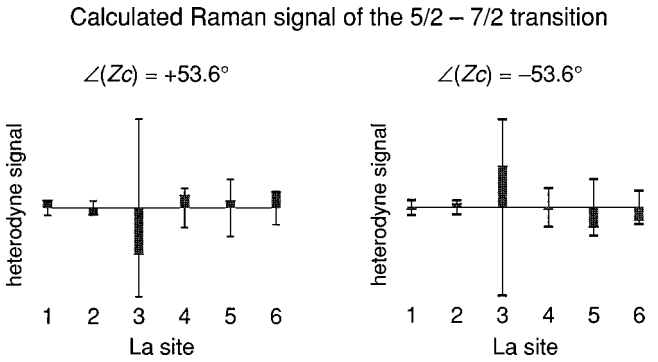

FIG. 10. Calculated intensity of the Raman heterodyne signal of the 5/2–7/2 transition as a function of the position of the neighboring La (site 1–6) and the orientation of the La EFG tensor. Thin lines indicate the maximum possible signal amplitude at each site. Thick bars are the intensity calculated for the two possible EFG orientations of the bulk La. The two possible angles of the Z axis of the tensor are $+53.6°$ from the c axis (left-hand side) and $-53.6°$ (right-hand side). The z axis of the Pr EFG tensor is $+81.4°$ from the crystal c axis.

VI. CONCLUSION

NQR transitions of La around Pr^{3+} in LaF_3 were observed as coherent Raman scattering resonant with the optical transition of Pr^{3+}. The signal arises from the magnetic interaction between the Pr and La nuclei. This superhyperfine effect had already been observed as sidebands of ODMR signals of Pr NQR by Macfarlane and Shelby.[14] However, the linewidth of these sidebands is too broad to resolve the quadrupole splitting of neighboring La nuclei. The linewidth is determined by the Pr dipolar width of 160 kHz. On the other hand, the linewidth of the coherent Raman NQR is the intrinsic La dipolar width of 10 kHz. The intensity of the NQR Raman signal of La is about 600 times smaller than that of Pr.[10] However, as in the first application of the Raman heterodyne technique to the superhyperfine spectra of Al around Cr^{3+} in ruby,[27] the high sensitivity of the technique made it possible to identify five different environments. From the observation the quadrupole parameters of the local La atoms are determined. As for the orientation of the local EFG, experiments in an external magnetic field would bring detailed information. Further experiments are planned in that direction. We hope that the present work demonstrates the potential of the technique to study weak interaction and local environments in solids and that the technique will be employed in studies of other systems.

ACKNOWLEDGMENTS

The authors are indebted to Dr. Y. Takahashi in Kyoto University for kindly lending us the crystals. M.M. is grateful to Professor D. Suter for helpful discussions. The work was partially supported by a Grant-in-Aid for Scientific Research from the Ministry of Education, Science, Sports and Culture in Japan (07454158 and 08740471). M.M. wishes to acknowledge Asahi Glass Foundation for a research grant.

*Electronic address: michio@ims.ac.jp.
†Present address: TAKARA Inc. Osaka, 541-0057, Japan.

[1] J. A. Giordmaine and W. Kaiser, Phys. Rev. **144**, 676 (1966).
[2] J. Mlynek, N. C. Wong, R. G. DeVoe, E. S. Kintzer, and R. G. Brewer, Phys. Rev. Lett. **50**, 993 (1983).
[3] N. C. Wong, E. S. Kintzer, J. Mlynek, R. G. DeVoe, and R. G. Brewer, Phys. Rev. B **28**, 4993 (1983).
[4] D. R. Taylor, Opt. Commun. **52**, 204 (1984).
[5] M. Mitsunaga, E. S. Kintzer, and R. G. Brewer, Phys. Rev. B **31**, 6947 (1985).
[6] E. S. Kintzer, M. Mitsunaga, and R. G. Brewer, Phys. Rev. B **31**, 6958 (1985).
[7] Y. Takahashi, K. Ishikawa, Y. Fukuda, T. Yabuzaki, and T. Hashi, Phys. Rev. B **43**, 7527 (1991).
[8] T. Blasberg and D. Suter, Phys. Rev. B **51**, 12 439 (1995).
[9] Y. Takahashi, K. Ishikawa, T. Tanaka, Y. Fukuda, H. Hatanaka, and T. Hashi, Phys. Rev. B **38**, 7121 (1988).
[10] M. Matsushita and T. Kato, Chem. Phys. Lett. **273**, 291 (1997).
[11] I. Oftedal, Z. Phys. Chem. Abt. B **5**, 272 (1929).
[12] B. Maximov and H. Schulz, Acta Crystallogr., Sect. B: Struct. Sci. **41**, 88 (1985).
[13] A. Zalkin and D. H. Templeton, Acta Crystallogr., Sect. B: Struct. Sci. **41**, 91 (1985).
[14] R. M. Macfarlane and R. M. Shelby, in *Spectroscopy of Solids Containing Rare Earth Ions*, edited by A. A. Kaplyanskii and R. M. Macfarlane (North-Holland, Amsterdam, 1987), pp. 51–184.
[15] M. A. Teplov, Zh. Eksp. Teor. Fiz. **53**, 1510 (1967) [Sov. Phys. JETP **26**, 872 (1968)].
[16] B. R. Reddy and L. E. Erickson, Phys. Rev. B **27**, 5217 (1983).
[17] Y. C. Chen, K. Chiang, and S. R. Hartmann, Phys. Rev. B **21**, 40 (1980).
[18] M. Dahl and G. Schaack, Z. Phys. B **56**, 279 (1984).
[19] A. Zalkin, D. H. Templeton, and T. E. Hopkins, Inorg. Chem. **5**, 1466 (1966).
[20] L. O. Andersson and W. G. Proctor, Z. Kristallogr. **127**, 366 (1968).
[21] Y. Takahashi, T. Hashi, and Y. Fukuda, Phys. Rev. A **48**, 2995 (1993).
[22] T. W. Hansch and B. Couillaud, Opt. Commun. **35**, 441 (1980).
[23] K. Lee, A. Sher, L. O. Andersson, and W. G. Proctor, Phys. Rev. **150**, 168 (1966).
[24] R. M. Shelby, R. M. Macfarlane, and C. S. Yannoni, Phys. Rev. B **21**, 5004 (1980).
[25] M. J. Weber, J. Chem. Phys. **48**, 4774 (1968).
[26] L. E. Erickson, Phys. Rev. B **42**, 3789 (1990).
[27] A. Szabo, T. Muramoto, and R. Kaarli, Opt. Lett. **13**, 1075 (1988).